Journal of Catalysis 375 (2019) 371–379

Contents lists available at ScienceDirect

Journal of Catalysis

journal homepage: www.elsevier.com/locate/jcat

Enhancing catalytic performance via structure core-shell metal-organic frameworks

Yanyan Gong [a,b], Ye Yuan [a], Cheng Chen [a], Pan Zhang [a,b], Jichao Wang [a,b], Anish Khan [e], Serge Zhuiykov [d], Somboon Chaemchuen [a,c,*], Francis Verpoort [a,b,c,d,*]

[a] Laboratory of Organometallics, Catalysis and Ordered Materials, State Key Laboratory of Advanced Technology for Materials Synthesis and Processing, Wuhan University of Technology, Wuhan 430070, PR China
[b] School of Materials Science and Engineering, Wuhan University of Technology, Wuhan 430070, PR China
[c] National Research Tomsk Polytechnic University, Lenin Avenue 30, 634050 Tomsk, Russian Federation
[d] Ghent University, Global Campus Songdo, 119 Songdomunhwa-Ro, Yeonsu-Gu, Incheon, Republic of Korea
[e] Center of Excellence for Advanced Materials Research, King Abdulaziz University, P.O. Box 80203, Jeddah 21589, Saudi Arabia

ARTICLE INFO

Article history:
Received 23 March 2019
Revised 5 June 2019
Accepted 15 June 2019

Keywords:
MOF@MOF
Core-shell structure
Heterogeneous catalysis
Knoevenagel condensation
MOFs

ABSTRACT

A core-shell structure metal-organic framework based on the Zr clusters bridging with BDC linkers (UiO-66) as a core-structure and BPYDC linkers (UiO-67-BPY) as a shell-structure was developed (UiO-67-BPY@UiO-66). The combination of several techniques *such as* XRD, FTIR, SEM, TEM, and surface area analysis etc. were applied for the characterization and confirmed a core-shell structure of UiO-67-BPY@UiO-66. Taking advantage of the high porous stability of the core-structure (UiO-66) and the presence of active Lewis basic sites from the bipyridinic linker in the shell layer (UiO-67-BPY) could be advantageous for basic-catalyzed reactions. The synthesized core-shell material was applied as a heterogeneous catalyst for the Knoevenagel condensation as a model reaction. An excellent catalytic performance was obtained by the core-shell material over traditional MOFs and other previous reports based on MOFs. The excellent dispersion of the active sites (Lewis basic) in the outer layer of the designed core-shell structure was a breakthrough to prevent mass diffusion limitation during catalysis. Additionally, the catalyst can be recycled and maintained its high catalytic performance at least for four cycles.

1. Introduction

In the class of porous crystalline materials, Metal-organic Frameworks (MOFs), constructed from metal ions or clusters and organic ligands possessing an infinite network, are currently receiving considerable attention. These MOFs exist as porous framework materials and possess outstanding properties for example high surface area, inherent porosity, multiple coordination sites, ease of functionalization, well-defined structures, and tunable pores size and volume etc. These materials are applied in multiple fields *such as* gas storage [1], separation [2], chemical sensing [3], catalysis [4–7], and drug delivery [8,9]. The post-synthetic modification is a strategy to enhance or access diversities of applications of MOF materials. Other strategies typically involve modification of either ligands or metal clusters to meet some particular requirements. However, still many difficulties arise using the traditional MOFs methodology. Thereby, explorations to increase the structural and functional complexity of MOFs to form multifunctional, purpose-designed MOFs is still developing at a high pace [10,11]. One kind of these explorations is the implementation of the core-shell strategy where MOF is encapsulated within another MOF generating a multifunctional hybrid MOF material, denoted as MOF@MOF [12,13]. The hybrid MOF@MOF materials may combine individual functions of core- and/or shell-MOF to exhibit novel synergetic chemical and physical properties suitable for selected applications [14–16]. For example, Lee et al. reported a core-shell nanocomposite ZIF-L@ZIF-8 through heterogeneous surface growth applied for CO_2 adsorption [17]. The realization of dynamic and equilibrium CO_2 adsorption characteristics were found on the core-shell material and presented a hybridized CO_2 uptake and diffusivity of parent crystals. Ren et al. fabricated core-shell nanocrystals MIL-101@UiO-66 which exhibited a high degree of moisture tolerance and hydrogen storage capacity 26%

* Corresponding authors at: Laboratory of Organometallics, Catalysis and Ordered Materials, State Key Laboratory of Advanced Technology for Materials Synthesis and Processing, Wuhan University of Technology, Wuhan 430070, PR China.
E-mail addresses: sama_che@hotmail.com (S. Chaemchuen), francis.verpoort@ghent.ac.kr (F. Verpoort).

https://doi.org/10.1016/j.jcat.2019.06.031
0021-9517/

and 60% higher than that of the individual MIL-101 and UiO-66, respectively [18]. Hirai et al. demonstrated the design of core-shell $Zn_2(bdc)_2$-$(dabco)_n$@$Zn_2(adc)_2(dabco)_n$ which could extract cetane from its branched isomer even at a low concentration of cetane (<1%). This separation could not be demonstrated independently by either traditional core- or shell-MOFs [19].

The Knoevenagel condensation between activated methylene compounds and aldehydes is a significant classic reaction. This reaction provides a C—C coupling enabling the preparation of substituted alkenes, coumarin derivatives, applied in cosmetics, perfumes, polymers, and pharmaceuticals [20–24]. This reaction is traditionally catalyzed by alkali metal hydroxides or bases like primary, secondary, tertiary amines [25–28] and ammonium salts [29] under homogeneous conditions. Unfortunately, these catalysts are difficult to separate and to recover and consequently generate large amounts of waste. Hence, there is an existing need for the development of heterogeneous catalysts with evident advantages like suppressed side reactions, simple separation process, less corrosiveness and reusability with high turn-over number resulting in better selectivity and yield. Metal-organic frameworks (MOFs) as novel crystalline materials with tunable structure and properties have been identified as promising heterogeneous catalysts for the Knoevenagel condensation [30–34]. Previous reports by Seo et al. [35], Park et al. [36], and Hasegawa et al. [37] have demonstrated that the implementation of a pyridyl group and amide groups in the organic ligand could generate MOFs acting as basic catalysts.

Keeping in mind all those considerations, herein, we synthesized a core-shell MOF@MOF using UiO-66 as a core-structure with UiO-67-BPY as the shell-structure. Incorporating dipyridyl groups (BPYDC), well known as basic sites, in the shell-structure which could be a promising approach for base-catalyzed reactions. The Knoevenagel condensation reaction of aldehydes with activated methylene compounds (malononitrile) was selected as a model reaction to evaluate the synthesized material as a heterogeneous catalyst. So far, the literature of MOF@MOF as a heterogeneous catalyst for this reaction is scarce. The synthesis route of the core-shell structured UiO-67-BPY@UiO-66 is demonstrated in Scheme 1. Firstly, UiO-66 (1,4-dicarboxybenzene (H_2bdc) as a ligand) as the core is synthesized and then UiO-67-BPY (2,2′-bipyridine-5,5′-dic arboxylic acid (H_2bpydc) is used as a ligand to grow the shell structure around the UiO-66 core.

2. Materials and methods

2.1. Materials preparation

2.1.1. Synthesis of UiO-66

All reagents were of analytical grade obtained from commercial suppliers (Sigma-Aldrich, Aladdin, and TCI) and used without further purification. The solvothermal synthesis of UiO-66 was conducted with a small modification of the reported procedure [38]. Briefly, the $ZrCl_4$ (0.17 g, 0.73 mmol) was dissolved in 20 mL of N, N-dimethylformamide (DMF) and sonicated for 15 min before adding 1,4-benzene dicarboxylic acid (H_2BDC, 0.12 g, 0.73 mmol). Thereafter, glacial acetic acid (1.25 mL) as a modulator was added to the solution with further sonication for 20 min. The obtained homogeneous solution was transferred into a 40 mL Teflon-lined stainless steel autoclave and heated to 120 °C for 24 h under autogenic pressure. After cooling to room temperature, the resultant white product was isolated by centrifugation and washed with DMF (3 × 10 mL), followed by immersion in methanol (MeOH) for 3 days and exchange with fresh MeOH every day. After immersion, the solids were collected and dried at 60 °C under vacuum for 24 h (activation) before further used.

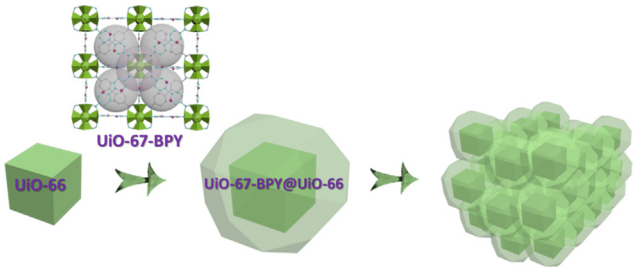

Scheme 1. Schematic diagram of the synthesis of core-shell UiO-67-BPY@UiO-66.

2.1.2. Synthesis of UiO-67-BPY

UiO-67-BPY was synthesized according to the formerly reported procedure [39]. Typically, $ZrCl_4$ (0.233 g, 1 mmol) was dissolved in 60 mL DMF under sonication for 15 min before 2,2′-bipyridine-5, 5′-dicarboxylic acid (H_2BPYDC, 0.244 g, 1 mmol) and 1.91 mL of glacial acetic acid were added. The mixture was sonicated further for 20 min and transferred into a 100 mL Teflon-lined stainless steel autoclave before heating to 120 °C for 24 h. After cooling to room temperature, the precipitate was isolated and washed similarly as the described procedure for UiO-66.

2.1.3. Synthesis of UiO-67-BPY@UiO-66

The powder of synthesized UiO-66 (80 mg), used as core-structure, was added to a mixture prepared from $ZrCl_4$ (46.6 mg, 0.2 mmol), H_2BPYDC (48.8 mg, 0.2 mmol), and glacial acetic acid (0.4 mL) in 25 mL DMF. The obtained suspension was transferred into a 40 mL Teflon-lined stainless steel autoclave and sonicated for 40 min before heating at 120 °C for 24 h. After cooling to room temperature, the product was collected by centrifugation and washed similarly as the described procedure for UiO-66.

2.2. Catalytic reaction

A 15 mL glass reactor was charged with aldehyde (1 mmol), malononitrile (1.2 mmol), DMSO-*d* (2 mL) and activated catalyst (18 mg) under ambient atmosphere. The mixture was stirred at room temperature (RT) for 1 h. After completion of the reaction, the suspension was centrifuged and the liquid phase was used to examine the conversion while the solid catalyst was recovered for further recycling tests.

2.3. Recycling procedure

After completion of the reaction, the catalyst was isolated by centrifugation and adequately washed with methanol (5 × 15 mL) before drying under vacuum at 80 °C for 24 h. Thereafter, the recovered catalyst was added to the reaction mixture for the next cycle applying reaction conditions described for the catalytic reaction.

2.4. Characterizations

The crystallinity of the samples was analyzed by powder XRD using a Bruker D8 advance diffractometer (Bragg-Brentano geometry) at 40 kV and 45 Ma with Cu-Kα radiation and a scanning rate of $0.1^\circ\,s^{-1}$. The size and morphology of the materials were investigated by using a field-emission scanning electron microscopy (FE-SEM, Zeiss Ultra Plus) with an X-Max 50 energy dispersive spectrometer (EDS) and a transmission electron microscopy (TEM, JEM-2100F). The surface area, porosity, and N_2 adsorption-desorption isotherms (77 K) were measurement on micrometrics instrument (ASAP 2020). Fourier transformed infrared spectra (FT-IR) were recorded on a Nicolet 6700 FT-IR spectrometer with KBr pellets in the range from 4000 to 400 cm^{-1}. The metal contents

were obtained by inductively coupled plasma optical emission spectrometry (ICP-OES, Prodigy 7). The CHN elements were analyzed by Element analysis (Vario EL cube). The reaction products were analyzed using a nuclear magmatic resonance (Bruker NMR 500 MHz). The acidic and basic properties of MOFs were examined via temperature programmed desorption (TPD) (AutoChem II 2920) using NH_3 and CO_2 as probe gases. Before TPD analysis, the sample was first placed inside the instrument and pretreated at 150 °C for 3 h under a He flow. The desorption process was temperature programmed (10 °C/min) and the signal was detected via a thermal conductivity detector (TCD).

3. Results and discussion

3.1. Characterization core-shell UiO-67-BPY@UiO-66

3.1.1. Morphology analysis

The UiO-67-BPY@UiO-66 MOFs was constructed to obtain the core-shell structure. Firstly, the Zr clusters bridging with 1,4-benzene dicarboxylic acid (H_2BDC) ligands (UiO-66) were synthesized as a core-structure followed by the addition of the second linker 2,2′-bipyridine-5,5′-dicarboxylic acid (BPYDC) with Zr clusters assembly to construct (UiO-67-BPY) the shell-structure. The morphology and crystal size of synthesized materials were determined via field emission scanning electron microscope (FE-SEM) and field emission transmission electron microscope (FE-TEM) analysis. The FE-SEM images demonstrated an octahedral shape morphology of UiO-66 with particle size ~150 nm (Fig. 1a), while the core-shell UiO-67-BPY@UiO-66 observed a spherical-like shape with particle size ~200 nm (Fig. 1d). The TEM images confirmed the achievement of a core-shell structure UiO-67-BPY@UiO-66 as additional layer coating (shell-structure of UiO-67-BPY) on UiO-66 crystal (Fig. 1e and f). Furthermore, a larger particle size of UiO-67-BPY@UiO-66 compared with the UiO-66 crystal size evidences the core-shell structure and further notifies about the thickness of the shell-layer UiO-67-BPY (~50 nm).

3.1.2. Crystallinity analysis

Powder X-ray diffraction (PXRD) was performed to evaluate the crystal structure of the synthesized materials and compared with the simulated crystal patterns. The observed PXRD pattern of synthesized UiO-66 and UiO-67-BPY (traditional structure core- and shell-MOFs) matched perfectly with their simulated patterns (Figs. S1 and S2). While the obtained crystal pattern of core-shell UiO-67-BPY@UiO-66 is in good agreement with the combination of the simulation of both structures UiO-66 and UiO-67-BPY. Moreover, not only a good agreement of the peak position but also of the intensity ratios were observed indicating a core-shell structure of the synthesized material (Fig. 2).

3.1.3. Functional group and porosity analysis

The existence of a core-shell structure was further examined by Fourier transform infrared spectroscopy (FTIR) as in Fig. S3. The bands located at 2500–3000 cm^{-1} represent characteristic bands of OH^- stretching vibration from organic ligands. These bands disappeared in the MOF structures due to the deprotonation of the organic linker followed by coordination with metal clusters during the framework construction [40,41]. Furthermore, a significant shift is observed for the C=O stretch vibration (1680 cm^{-1}) in the synthesized material compared to the free original ligand. The

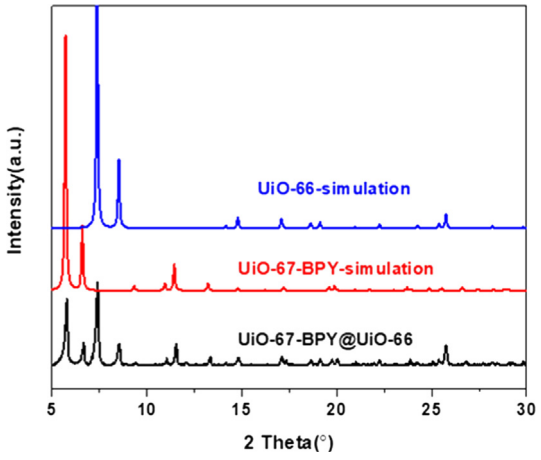

Fig. 2. The XRD pattern of as-synthesized UiO-67-BPY@UiO-66 compared with the simulated structure of UiO-66 and UiO-67-BPY.

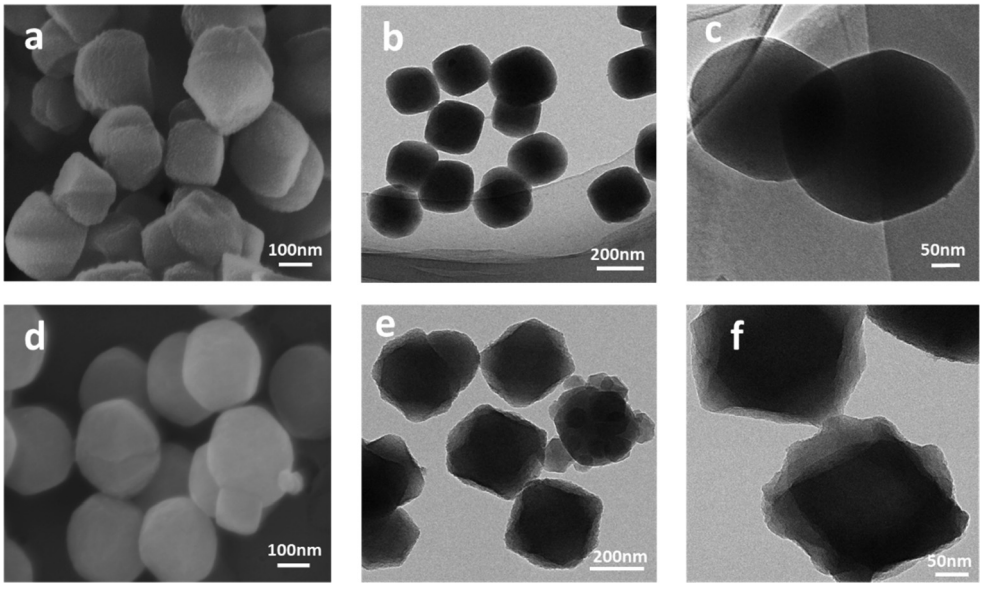

Fig. 1. The crystal morphology images of UiO-66 (a–c) and UiO-67-BPY@UiO-66 (d–f) *via* FE-SEM (a and d) and TEM (b, c, e and f).

characteristic bands centered at 1590 cm^{-1} and 1417 cm^{-1} were found in all three synthesized MOFs and are attributed to the carboxylic ligand in the framework of the MOFs [42–46,32]. Though the peaks observed at 1590 and 1417 cm^{-1} cannot be reliably assigned to the C=N stretching vibration of the dipyridyl groups of UiO-67-BPY@UiO-66, an increase in the intensity of these peaks in contrast to that of UiO-66 and UiO-67-BPY is observed and may be attributed to the C=N stretching mode of the dipyridyl from the shell layer. The nitrogen adsorption measurements at 77 K were performed on UiO-66, UiO-67-BPY, and UiO-67-BPY@UiO-66 and revealed an isotherm of *type I* for all samples. Moreover, a larger BET surface area and pore volume of UiO-67-BPY@UiO-66 (1470 $m^2 \cdot g^{-1}$ and 0.56 $cm^3 \cdot g^{-1}$) than UiO-66 (853 $m^2 \cdot g^{-1}$ and 0.33 $cm^3 \cdot g^{-1}$) was observed (Fig. 3). The higher surface area of the core-shell UiO-67-BPY@UiO-66 could be attributed to the additional larger porosity of the UiO-67-BPY shell (1700 $m^2 \cdot g^{-1}$) [39]. Additionally, the BET surface area of the core-shell material was located between those of UiO-66 and UiO-67-BPY as reported in previous studies [15,47,48].

3.1.4. Temperature-programmed desorption (TPD) and element analysis

The temperature-programmed desorption (TPD) using CO_2 and NH_3 as probe gases was applied to investigate the amount of basic and acid sites in the synthesized materials (Fig. 4). The CO_2 or NH_3 amount desorbed during temperature raising and the temperature range of desorption correspond to the concentration and the distribution of the strength of basic or acid sites, respectively. From the CO_2-TPD profile (Fig. 4a), two distinct CO_2 desorption peaks are observed and correspond to a different strength of the basic sites. The peak centered at ~300 °C was assigned to CO_2 molecules adsorption on basic sites with a moderate strength, whereas the peak positioned at ~710 °C was attributed to stronger interactions with CO_2 molecules and represent the strong basic sites [49–52]. The total amount of basic sites was integrated from the area under the curve for UiO-67-BPY@UiO-66 and UiO-67-BPY and revealed an amount of 634 μmol/g and 385 μmol/g, respectively. The amount of basic sites is of significance for the catalytic performance in the Knoevenagel condensation as will be discussed in the catalytic performance section. The NH_3-TPD patterns of the synthesized materials are displayed in Fig. 4b. Similar desorption profiles were found on both synthesized materials, though, the total amount of acid sites in UiO-67-BPY was larger than in UiO-67-BPY@UiO-66 (984 μmol/g and 556 μmol/g, respectively). Combining both TPD results, the UiO-67-BPY@UiO-66 MOF revealed a better acid-base balance, and consequently, a concerted and synergic action might take place during the reaction which is beneficial to increase the catalytic performance [53]. It could be inferred that there exist two kinds of acid sites with different acidic strengths. The peaks located at ~200 °C indicated the NH_3 molecules adsorbed at weak acid sites, while the other peak centered ~380 °C derives from NH_3 desorption from moderate acid sites [54–58]. Table 1 gives the results obtained from element analysis (C, H, N) and clearly indicates that the N content of the core-shell UiO-67-BPY@UiO-66 (3.43%) is lower than UiO-67-BPY (5.84%). Although the content of N is lower in the core-shell material, the amount of basic sites in the core-shell UiO-67-BPY@UiO-66 is higher than in UiO-67-BPY and could indicate that "more accessible" basic sites are present in the core-shell material. It has to be mentioned that the pyridyl groups of H_2BPYDC mainly generate the basic sites present in UiO-67-BPY and core-shell UiO-67-BPY@UiO-66. For this reason, an acid/base analysis of only those two materials was performed since UiO-66 lacks the basic sites.

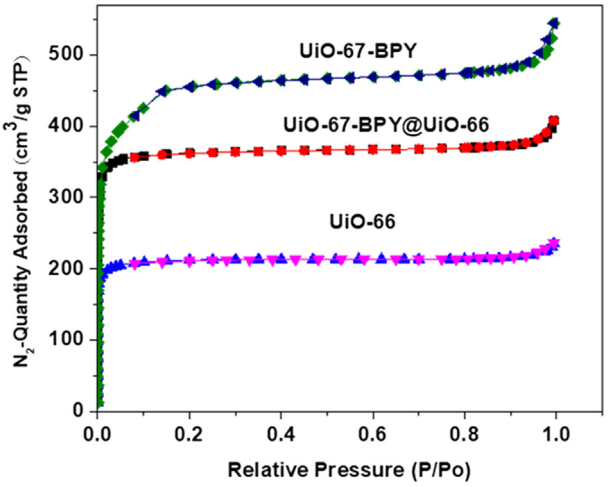

Fig. 3. The N_2 isotherms of UiO-66, UiO-67-BPY and UiO-67-BPY@UiO-66.

Table 1
Elemental analysis (C H N) results for different samples.

Sample	N %	C %	H %
Fresh UiO-67-BPY@UiO-66	3.43	31.65	3.13
UiO-67-BPY	5.84	31.57	3.05
Recovered UiO-67-BPY@UiO-66	3.41	32.93	2.84

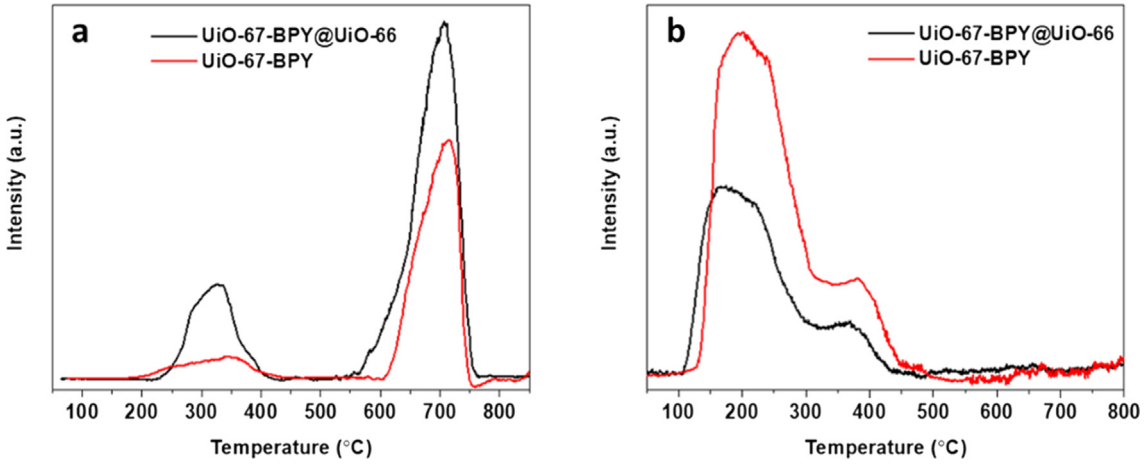

Fig. 4. The CO_2-TPD (a) and NH_3-TPD (b) profiles of UiO-67-BPY@UiO-66 and UiO-67-BPY.

3.2. Catalytic performance

The robust core-shell structure (MOFs@MOFs) is designed to eliminate the diffusion limitation that generally occurs in porous heterogeneous catalysts and thus also in MOFs. Definitively, well-dispersed active sites near the MOF surface could enhance the substrates to react with the active sites as well as provide a faster diffusion out of the pores of the product. The core-shell UiO-67-PBY@UiO-66 was applied as a heterogeneous catalyst for the Knoevenagel condensation of aldehydes with compounds containing active methylene groups. The conversion of benzaldehyde with malononitrile was used as a model reaction to evaluate the catalytic performance of the synthesized materials: UiO-66, UiO-67-PBY@UiO-66, and UiO-67-PBY. The discrepancy in catalytic performance of UiO-67-PBY@UiO-66 depends on the catalyst amount and reaction time as shown in Fig. 5 and Fig. S4. The conversion increased along with the catalyst loading as well as reaction time and conversion of up to 98% is obtained using 18 mg UiO-67-PBY@UiO-66 after 1 h reaction time. The core-shell MOFs also exhibited an excellent reactivity for the Knoevenagel condensation of benzaldehyde and malononitrile even in a short period of 20 min (83% conversion) or 40 min (95%).

The effect of the core-shell structure on the catalytic performance was investigated by comparing with the individual core- and shell-MOF under identical reaction conditions. The core-shell UiO-67-BPY@UiO-66 revealed the highest catalytic activity (98% conversion) followed by the shell UiO-67-BPY (87%) and the core UiO-66 with 25% conversion after 1 h. Furthermore, without a catalyst, this model reaction achieved a very low conversion (29%). Basically, the conversions obtained by UiO-66 and without catalyst are similar indicating that active sites (acid sites) in UiO-66 hardly promoted this reaction. The higher total amount of basic sites in the core-shell UiO-67-BPY@UiO-66 (see CO_2-TPD analysis) compared with UiO-67-BPY, seems to be the main cause for the higher catalytic performance. Interestingly, the core-shell UiO-67-BPY@UiO-66 catalyst contains a lower N content (3.43%) compared to UiO-67-BPY (5.84%) still, a higher reactivity was obtained. This clearly points out that the basic sites (N-atoms) in the core-shell structure are easily accessible and that diffusion is not limited. In addition, the FESEM images of UiO-67-BPY demonstrated a particle size of 1 μm (Fig. S5) similar as previous reported [39], which is considerably bigger than the core-shell MOF particles (200 nm). These findings clearly demonstrate that the synergy between the core and shell has a crucial effect on the catalytic activity.

In order to better understand the influence of core-shell structure on the catalytic performance of UiO-67-PBY@UiO-66 materials, small sized UiO-67-BPY particles (denoted as UiO-67-BPY-S, ~200 nm based on the FESEM images, Fig. S8) were synthesized via tuning of the synthesis conditions. The UiO-67-BPY-S has a similar particle size as compared with core-shell UiO-67-BPY@UiO-66 and was further used to investigate the influence of particle size on the catalytic performance. The results revealed a conversion of 61% (30 min) and 80% (60 min) (Fig. S8), which is still lower than the conversion obtained using core-shell UiO-67-BPY@UiO-66 catalyst under similar conditions.

In addition, as displayed in Table 3 (Entry 7–8), 4-tert-butylbenzaldehyde with large molecular size was used as the substrate to evaluate the effect of core-shell structure on catalytic activity. Yields of 75% and 55% were achieved for UiO-67-BPY@UiO-66 and UiO-67-BPY, respectively, confirming the excellent improved effect of core-shell structure on the catalytic activity.

The catalytic performance of core-shell UiO-67-BPY@UiO-66 for the Knoevenagel condensation of benzaldehyde and malononitrile was compared with previous reports based on MOF catalysts (Table 2). For more than half of the reported MOF catalysts harsh reaction conditions were needed which was indispensable for an appropriate conversion. Here in, the core-shell UiO-67-BPY@UiO-66 demonstrated an excellent conversion of benzaldehyde under milder reaction conditions (RT) and short time (1 h). The results fully reflect the excellent catalytic performance of the core-shell MOF compared to other MOF catalysts.

To demonstrate the capability the core-shell UiO-67-PBY@UiO-66 as a catalyst for the Knoevenagel condensation reaction the substrate scope using different aldehydes applying was investigated. Therefore, the catalytic performance using aromatic aldehydes with different electronic and steric substituents was explored (Table 3). For the benzaldehyde, up to 98% conversion was achieved after 1 h (Entry 1). Faster conversion rates were obtained for aldehydes with electron-withdrawing groups, which could reach completion within only 30 min (Entry 2–5). However, benzaldehyde with electron-donating groups (Entry 6–7) retarded the reaction rate and hence, a lower conversion was obtained after 1 h. Those results indicated that electron-withdrawing groups promote the reaction, as expected in this reaction based on the nucleophilic attack of the basic sites of the core-shell MOF at the carbonyl group of the aldehyde. The NMR spectra of the products obtained from the different aromatic aldehydes are depicted in Fig. S6.

3.3. Catalytic mechanism

A plausible catalytic mechanism only involving basic sites of the core-shell UiO-67-PBY@UiO-66 catalyst is given in Fig. S7 (left). In

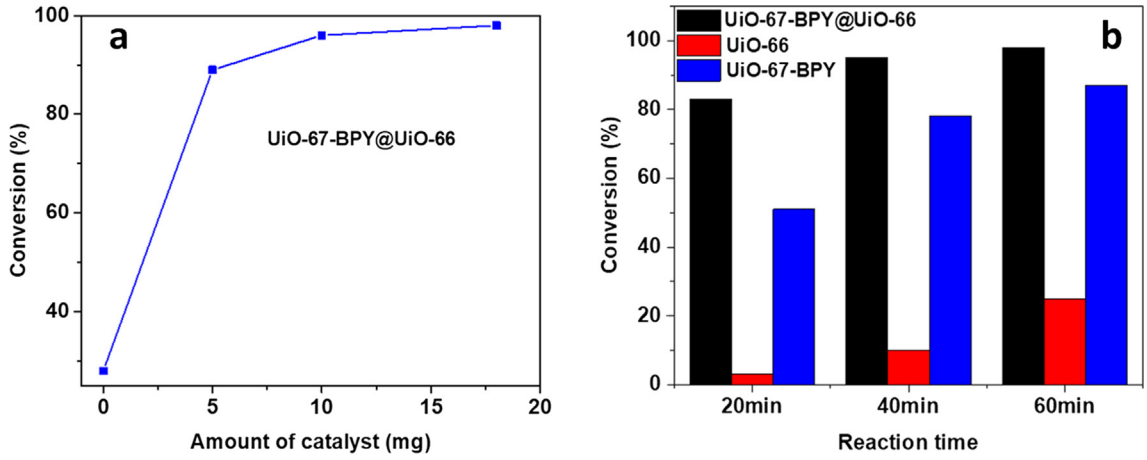

Fig. 5. The conversions of benzaldehyde after 1 h using different amounts of UiO-67-BPY@UiO-66 (0, 5, 10, 18 mg) (a) and the conversions of benzaldehyde using different MOFs after 20, 40, 60 min with 18 mg catalyst (b).

Table 2
Reported MOFs for the Knoevenagel condensation of benzaldehyde and malononitrile (model reaction).

Entry	Catalyst	T/°C	t/min	Yield	Ref.
1	UiO-66	100	270	5%	[59]
2	UiO-66-NH_2	100	240	13%	[59]
3	MIL-100 (Al)	100	270	30%	[59]
4	Cu-BTC	100	270	23%	[59]
5	Zn@ZIF-67	RT	90	50%	[34]
6	UiO-66-NH_2	40	40	98%	[60]
7	NH_2 (50%)-MIL-53	80	300	99%	[61]
8	MIL-53	80	300	87%	[61]
9	UiO-66-NH-RNH_2	RT	120	97%	[32]
10	CAU-1-NH_2	40	60	94%	[62]
11	ZIF-8	RT	180	100%	[63]
12	CuBTC	130	60	100%	[64]
13	FeBTC	130	180	100%	[64]
14	DETA-MIL-101	RT	60	97%	[65]
15	IRMOF-3	40	120	99%	[66]
16	Al-MIL-101-NH_2	80	30	61%	[67]
17	ZIF-9	RT	240	99%	[68]
18	UiO-67-BPY@UiO-66	RT	60	98%	This work

Table 3
The catalytic activity of UiO-67-BPY@UiO-66 using different aromatic aldehydes.[a]

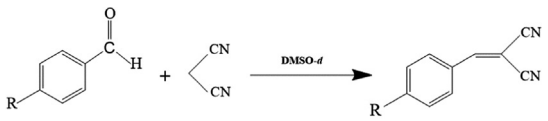

Entry	Substrate	T (°C)	t (min)	Conversion[b]
1	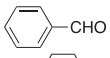	RT	60	98%
2	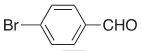	RT	30	100%
3	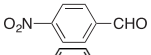	RT	30	100%
4	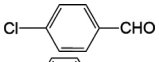	RT	30	100%
5	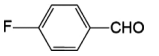	RT	30 60	92% 98%
6	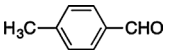	RT	60 120	88% 96%
7	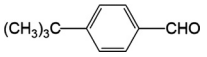	RT	60	75%
8	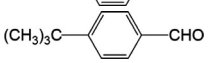 (UiO-67-BPY as catalyst)	RT	60	55%

[a] Reaction conditions: aldehyde (1 mmol), malononitrile (1.2 mmol), catalyst (18 mg), DMSO-*d* (2 mL), room temperature (RT).
[b] The conversions of aldehydes were determined by ^{1}H NMR analysis.

the reaction mechanism, an H-atom of the methylene group in malononitrile is abstracted by the basic sites, producing a carbanion. Then a nucleophilic attack of the carbanion on the carbon atom of the carbonyl group from the aldehyde gives the intermediate. Finally, after an appropriate rearrangement together with a dehydration process, the condensation product is generated [44–46,59,69,70]. The catalytic mechanism is related only to the basic sites of the core-shell UiO-67-BPY@UiO-66. This could be stated from the fact that low conversions were obtained for the reaction with UiO-66 (contains only acid sites) and the reaction without a catalyst. These results indicate that the acid sites in UiO-66 had no effect on the reactivity [32]. Furthermore, when using dipyridyl (only containing basic sites) as a homogeneous catalyst for this Knoevenagel condensation reaction of benzaldehyde and malononitrile, the product was generated as demonstrated in Fig. S7 (right). These two pieces of evidence proved that the mechanism during the reaction might only involve the basic sites of the catalyst.

As we demonstrated that only the basic sites play a role in the catalysis, a catalytic mechanism using the basic sites of the core-shell UiO-67-BPY@UiO-66 is proposed. Herein, the N present in the bipyridine linker (H_2BPYDC) offers the basic sites for the catalytic system. In principle, it is believed that a higher N loading could provide a higher catalytic activity for base-catalyzed reaction. However, the opposite phenomenon was observed in this work, a lower N content of the core-shell UiO-67-BPY@UiO-66 (N content 3.43%wt, ICP) exhibited a higher reactivity than UiO-67-BPY (N content 5.84%wt, ICP). Additionally, the molecular dimension of benzaldehyde (6.0×4.3 Å), malononitrile (2.8×4.3 Å) and the product benzylidenemalononitrile (3.7×7.7 Å) are smaller than the pore sizes of UiO-67-BPY@UiO-66 (13.01 Å) and UiO-67-BPY (13.07 Å), so these species can enter inside the pores of both catalysts. However, the higher reactivity of the core-shell UiO-67-BPY@UiO-66 can be explained by the higher total amount of basic sites in the core-shell MOFs as mentioned in TPD analysis in addition to a synergistic effect of the core-shell structure for the diffusion rate of substrate and/or product molecules through the pores of the shell of the core-shell catalyst. Compared with UiO-67-BPY@UiO-66, due to the large particle size of UiO-67-BPY (1 μm), the substrate and product molecules might experience a difficult diffusion through the pores. Finally, due to a larger particle size of UiO-67-BPY, a smaller surface interaction between the substrate and the active sites will occur. Those reasons might imply that the accessibility of the active sites inside of UiO-67-BPY is limited by diffusion difficulties of the substrate and/or product molecules. Whereas, the diffusion issues in the shell layer UiO-67-BPY of the core-shell UiO-67-BPY@UiO-66 structure having a smaller thickness (50 nm) were prevented. Since the diffusion was avoided in the core-shell structure a higher catalytic performance could be observed for the Knoevenagel condensation of benzaldehyde and malononitrile even at short reaction time.

3.4. Reusability UiO-67-PBY@UiO-66

An important property of a heterogeneous catalyst is the catalyst recyclability and stability. The obtained results of reusability study of the core-shell UiO-67-PBY@UiO-66 heterogeneous catalyst is given in Fig. 6. Therefore, after the completion of the reaction, the catalyst UiO-67-PBY@UiO-66 was isolated from the reaction mixture by centrifugation, washed with plenty of methanol, and finally dried at 80 °C for 24 h under vacuum. The catalyst was recovered and reused in successive runs for the Knoevenagel condensation with a small loss in catalytic activity after four recycles. The spent catalyst was characterized on its crystal morphol-

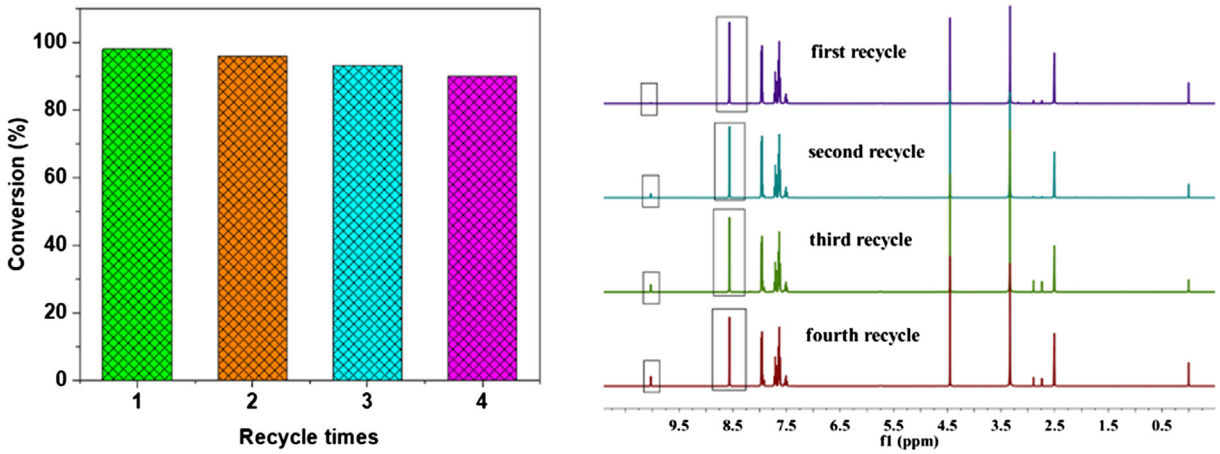

Fig. 6. The recycling performance (left) and ^{1}H NMR spectra (right) of the reaction mixture for the Knoevenagel condensation of benzaldehyde and malononitrile using UiO-67-BPY@UiO-66 (at room temperature; reaction time: 1 h).

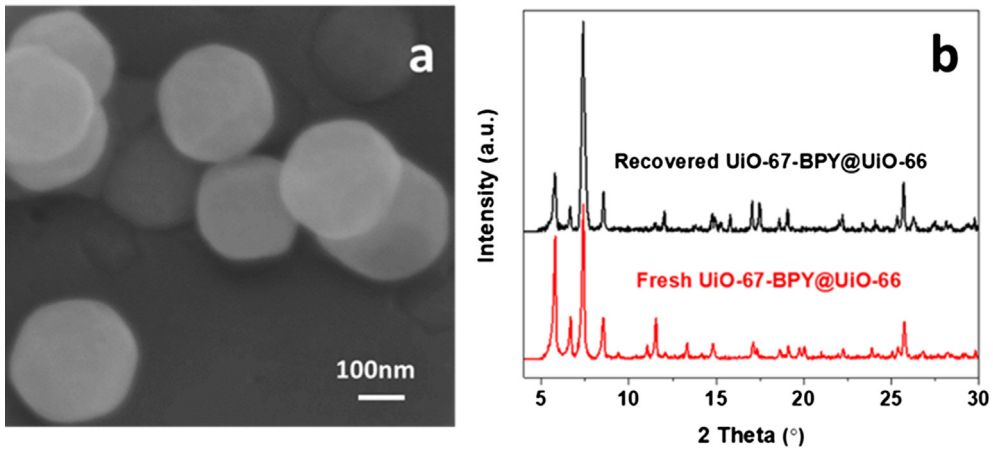

Fig. 7. The FESEM images (a) and PXRD patterns of core-shell catalyst after reaction (b).

ogy, crystallinity and porosity via TEM, SEM, PXRD, and N_2 adsorption at 77 K, respectively (The new results are applied in the revised manuscript). The FESEM image (Fig. 7) shows that the size and morphology of the catalyst were almost completely preserved after the reaction. The N_2 isotherms revealed a slightly decreased adsorption which represents a small reduction of the surface area from 1470 $m^2 \cdot g^{-1}$ of the fresh catalyst to 1244 $m^2 \cdot g^{-1}$ of the spent catalyst (Fig. S9). The PXRD pattern (Fig. 7) of spent UiO-67-BPY@UiO-66 definitely exhibits peaks of UiO-67-BPY ($2\theta = 5.8$, 6.7), however, the intensity of those peaks reduces relatively compared to the peaks of UiO-66 ($2\theta = 7.4$, 8.5). Additionally, the TEM images (Fig. S9) of the spent catalyst display a similar size and morphology compared with the fresh catalyst except for the irregular edges of the crystal particles, which could indicate a small degree of degradation of the catalyst after the reaction. Consequently, these results could represent a small loss in shell-structure (UiO-67-BPY) after the catalytic reaction. Nevertheless, the shell structure was generally preserved on the UiO-67-BPY@UiO-66 catalyst as confirmed by the similar particle size obtained from SEM and TEM images (Fig. 7 and Fig. S9). Additionally, the elemental analysis of N-species revealed a similar N content on fresh and spent catalyst and the absence of leached Zr in the solution. In parallel, the recovered core-shell catalyst was examined by element analysis (C, H, N) and the N-content revealed a neglectable change (3.41% for recovered, 3.43% for fresh), which proved the relatively stable structure of UiO-67-PBY@UiO-66.

4. Conclusions

A core-shell UiO-67-BPY@UiO-66 was successfully synthesized and exhibited excellent catalytic performance for the Knoevenagel condensation of aldehydes with malononitrile. Interestingly, the core-shell structure exhibited a higher catalytic performance over traditional core- and shell-MOFs (UiO-66 and UiO-67-BPY, respectively). The basic sites in the shell are key for the catalytic performance. The shell structure is of key importance to avoid diffusion issues. Moreover, the catalyst could be reused for at least four cycles with a small loss in catalytic performance. The synergistic effect between the core-shell structures was suggested to enhance their properties. The present work potentially promotes the development of novel high-performance heterogeneous catalytic systems by forming a core-shell structure. Further work is in progress to broaden the extent of application of this heterogeneous catalyst for other organic transformations.

Author contributions

Y.Y.G., S.C., and F.V. conceived the original idea and designed the experimental program. Y.Y.G. synthesized all the materials, carried out all the reactions, and some characterizations. P.Z. and J.C.W. performed part of BET and XRD analyses. C.C. and Y.Y. characterized reaction mixtures via NMR. S.C. and F.V. supervised the pro-

ject. Y.Y.G. wrote the initial draft of the manuscript. S.C. and F.V. finalized the draft version. All authors approved the final version of the manuscript.

Declaration of Competing Interest

The authors declare no competing financial interest.

Acknowledgement

The authors are grateful to the State Key Lab of Advanced Technology for Materials Synthesis and Processing for financial support (Wuhan University of technology). S.C. acknowledges the support of the National Natural Science Foundation of China (No. 21502146). F.V. appreciates the financial support from Tomsk Polytechnic University Competitiveness Enhancement Program grant (VIU-2019).

Appendix A. Supplementary material

General information, some supplementary characterization analysis and NMR characterization of products obtained from different aldehydes. Supplementary data to this article can be found online at https://doi.org/10.1016/j.jcat.2019.06.031.

References

[1] Y.H. Hu, L. Zhang, Hydrogen Storage in Metal-Organic Frameworks, Adv. Mater. 22 (2010).
[2] C.X. Yang, Y.J. Chen, H.F. Wang, X.P. Yan, High-performance separation of fullerenes on metal-organic framework MIL-101(Cr), Chemistry 17 (2011) 11734–11737.
[3] Z.Q. Li, L.G. Qiu, W. Wang, T. Xu, Y. Wu, X. Jiang, Fabrication of nanosheets of a fluorescent metal–organic framework $[Zn(BDC)(H_2O)]_n$ (BDC = 1,4-benzenedicarboxylate): Ultrasonic synthesis and sensing of ethylamine, Inorg. Chem. Commun. 11 (2008) 1375–1377.
[4] N.T.S. Phan, K.K.A. Le, T.D. Phan, MOF-5 as an efficient heterogeneous catalyst for Friedel-Crafts alkylation reactions, Appl. Catal. A-Gen. 382 (2010) 246–253.
[5] L.T.L. Nguyen, T.T. Nguyen, K.D. Nguyen, N.T.S. Phan, Metal–organic framework MOF-199 as an efficient heterogeneous catalyst for the aza-Michael reaction, Appl. Catal. A-Gen. 425–426 (2012) 44–52.
[6] N.T.S. Phan, T.T. Nguyen, C.V. Nguyen, T.T. Nguyen, Ullmann-type coupling reaction using metal-organic framework MOF-199 as an efficient recyclable solid catalyst, Appl. Catal. A-Gen. 457 (2013) 69–77.
[7] E. Rahmani, M. Rahmani, Al-based MIL-53 metal organic framework (MOF) as the new catalyst for Friedel-crafts alkylation of benzene, Ind. Eng. Chem. Res. 57 (2017) 169–178.
[8] K. Deng, Z. Hou, X. Li, C. Li, Y. Zhang, X. Deng, Z. Cheng, J. Lin, Aptamer-mediated up-conversion Core/MOF shell nanocomposites for targeted drug delivery and cell imaging, Sci. Rep.-Uk 5 (2015) 7851.
[9] Q.L. Li, J.P. Wang, W.C. Liu, X.Y. Zhuang, J.Q. Liu, G.L. Fan, B.H. Li, W.N. Lin, J.H. Man, A new (4,8)-connected topological MOF as potential drug delivery, Inorg. Chem. Commun. 55 (2015) 8–10.
[10] S.T. Meek, J.A. Greathouse, M.D. Allendorf, Metal-organic frameworks: a rapidly growing class of versatile nanoporous materials, Adv. Mter. 23 (2011) 249–267.
[11] S.M. Cohen, Postsynthetic methods for the functionalization of metal-organic frameworks, Chem. Rev. 112 (2012) 970–1000.
[12] K. Koh, A.G. Wongfoy, A.J. Matzger, MOF@MOF: microporous core-shell architectures, Chem. Commun. 41 (2009) 6162.
[13] S. Furukawa, K. Hirai, K. Nakagawa, Y. Takashima, R. Matsuda, T. Tsuruoka, M. Kondo, R. Haruki, D. Tanaka, H. Sakamoto, Heterogeneously hybridized porous coordination polymer crystals: fabrication of heterometallic core-shell single crystals with an in-plane rotational epitaxial relationship, Angew. Chem. Int. Edit. 48 (2010) 1766–1770.
[14] T. Fukushima, S. Horike, H. Kobayashi, M. Tsujimoto, S. Isoda, M.L. Foo, Y. Kubota, M. Takata, S. Kitagawa, Modular design of domain assembly in porous coordination polymer crystals via reactivity-directed crystallization process, J. Am. Chem. Soc. 134 (2012) 13341–13347.
[15] J. Zhuang, L.Y. Chou, B.T. Sneed, Y. Cao, P. Hu, L. Feng, C.K. Tsung, Surfactant-mediated conformal overgrowth of core-shell metal-organic framework materials with mismatched topologies, Small 11 (2015) 5551–5555.
[16] T. Li, J.E. Sullivan, N.L. Rosi, Design and preparation of a core-shell metal-organic framework for selective CO_2 capture, J. Am. Chem. Soc. 135 (2013) 9984.
[17] W.C. Lee, H.T. Chien, Y. Lo, H.C. Chiu, T.P. Wang, D.Y. Kang, Synthesis of zeolitic imidazolate framework core-shell nanosheets using zinc-imidazole pseudopolymorphs, Acs Appl. Mater. Inter. 7 (2015) 18353–18361.
[18] J. Ren, N.M. Musyoka, H.W. Langmi, B.C. North, M. Mathe, X. Kang, Fabrication of core-shell MIL-101(Cr)@UiO-66(Zr) nanocrystals for hydrogen storage, Int. J. Hydrogen Energy 39 (2014) 14912–14917.
[19] K. Hirai, S. Furukawa, M. Kondo, H. Uehara, O. Sakata, S. Kitagawa, Sequential functionalization of porous coordination polymer crystals, Angew. Chem. Int. Edit. 50 (2011) 8057–8061.
[20] A. Song, X. Wang, K.S. Lam, A convenient synthesis of coumarinarboxylic acids via knoevenagel condensation of meldrum′s acid with orthodroxyaryl aldehydes or ketones, Tetrahedron. Lett. 44 (2003) 1755–1758.
[21] F. Bigi, L. Chesini, R. Maggi, G. Sartori, ChemInform abstract: montmorillonite KSF as an inorganic, water stable, and reusable catalyst for the knoevenagel synthesis of coumarin-3-carboxylic acids, J. Org. Chem. 64 (1999) 1033–1035.
[22] A. Giseop Kwak, Michiya Fujiki, Colored and luminous aliphatic polyester via one-pot intra- and intermolecular knoevenagel reactions, Macromolecules 37 (2008) 2021–2025.
[23] F. Liang, Y.J. Pu, T. Kurata, J. Kido, H. Nishide, Synthesis and electroluminescent property of poly(p-phenylenevinylene)s bearing triarylamine pendants, Polymer 46 (2005) 3767–3775.
[24] L.F. Tietze, Domino reactions in organic synthesis, Chem. Rev. 96 (1996) 115–136.
[25] S. Balalaie, M. Bararjanian, Tetra-n-butylammonium hydroxide (TBAH)-catalyzed knoevenagel condensation: a facile synthesis of α-cyanoacrylates, n-cyanoacrylonitriles, and d-cyanoacrylamides, Synthetic. Commun. 36 (2006) 533–539.
[26] G. Cardillo, S. Fabbroni, L. Gentilucci, M. Gianotti, A. Tolomelli, A straightforward method for the synthesis of alkylidene and arylidene malonates through proline-catalyzed knoevenagel condensation, Synthetic. Commun. 33 (2003) 1587–1594.
[27] D.S. Acker, W.R. Hertler, Substituted quinodimethans. I. Preparation and chemistry of 7,7,8,8-Tetracyanoquinodimethan, J. Am. Chem. Soc. 84 (1962) 3370–3374.
[28] A.V. Narsaiah, A.K. Basak, B. Visali, K. Nagaiah, An eco-friendly synthesis of electrophilic alkenes catalyzed by dimethylaminopyridine under solvent-free conditions, Synthetic. Commun. 34 (2004) 2893–2901.
[29] E.J.C. Jr, C.M. Robb, J.M. Sprague, The synthesis of α, α-disubstituted succinic acids from ethyl alkylidenecyanoacetates, J. Org. Chem. 15 (1950) 381–390.
[30] Z. Miao, Y. Luan, C. Qi, D. Ramella, The synthesis of a bifunctional copper metal organic framework and its application in the aerobic oxidation/Knoevenagel condensation sequential reaction, Dalton. T. 45 (2016) 13917.
[31] Y. Zhang, Y. Wang, L. Liu, N. Wei, M.L. Gao, D. Zhao, Z.B. Han, Robust bifunctional lanthanide cluster based metal-organic frameworks (MOFs) for tandem deacetalization-knoevenagel reaction, Inorg. Chem. 57 (2018) 2193.
[32] Y. Luan, Y. Qi, H. Gao, R.S. Andriamitantsoa, N. Zheng, G. Wang, A general post-synthetic modification approach of amino-tagged metal–organic frameworks to access efficient catalysts for the Knoevenagel condensation reaction, J. Mater. Chem. A 3 (2015) 17320–17331.
[33] A.R. Burgoyne, R. Meijboom, Knoevenagel condensation reactions catalysed by metal-organic frameworks, Catal. Lett. 143 (2013) 563–571.
[34] A. Zanon, S. Chaemchuen, F. Verpoort, Zn@ZIF-67 as catalysts for the knoevenagel condensation of aldehyde derivatives with malononitrile, Catal. Lett. 147 (2017) 2410–2420.
[35] J.S. Seo, D. Whang, H. Lee, S.I. Jun, J. Oh, Y.J. Jeon, K. Kim, A homochiral metal-organic porous material for enantioselective separation and catalysis, Nature 404 (2000) 982–986.
[36] J. Park, J.R. Li, Y.P. Chen, J. Yu, A.A. Yakovenko, Z.U. Wang, L.B. Sun, P.B. Balbuena, H.C. Zhou, A versatile metal-organic framework for carbon dioxide capture and cooperative catalysis, Chem. Commun. 48 (2012) 9995–9997.
[37] S. Hess, J.W. Polak, A. Daly, G. Hyman, Three-dimensional porous coordination polymer functionalized with amide groups based on tridentate ligand: selective sorption and catalysis, J. Am. Chem. Soc. 129 (2007) 2607–2614.
[38] J.J. Zhou, R. Wang, X.L. Liu, F.M. Peng, C.H. Li, F. Teng, Y.P. Yuan, In situ growth of CdS nanoparticles on UiO-66 metal-organic framework octahedrons for enhanced photocatalytic hydrogen production under visible light irradiation, Appl. Surf. Sci. 346 (2015) 278–283.
[39] H. Fei, S.M. Cohen, A robust, catalytic metal-organic framework with open 2,2′-bipyridine sites, Chem. Commun. 50 (2014) 4810–4812.
[40] B. Mortada, T.A. Matar, A. Sakaya, H. Atallah, Z. Kara Ali, P. Karam, M. Hmadeh, Postmetalated zirconium metal organic frameworks as a highly potent bactericide, Inorg. Chem. 56 (2017) 4739–4744.
[41] C.I. Ezugwu, B. Mousavi, M.A. Asraf, Z. Luo, F. Verpoort, Post-synthetic modified MOF for Sonogashira cross-coupling and Knoevenagel condensation reactions, J. Catal. 344 (2016) 445–454.
[42] J.Q. Wang, L. Huang, M. Xue, Architecture of a hybrid mesoporous chemosensor for Fe^{3+} by covalent coupling bis-schiff base PMBA onto the CPTES-functionalized SBA-15, J. Phys. Chem. C 112 (2008) 5014–5022.
[43] H. Jin, Y. Qi, E. Wang, Molecular and multidimensional organic– inorganic hybrids based on polyoxometalates and copper coordination polymer with mixed 4, 4′-bipyridine and 2, 2′-bipyridine ligands, Cryst. Growth. Des. 6 (2006) 2693–2698.
[44] X. Dong, Y. Hui, S. Xie, P. Zhang, G. Zhou, Z. Xie, Schiff base supported MCM-41 catalyzed the Knoevenagel condensation in water, Rsc Adv. 3 (2013) 3222.

[45] F. Farzaneh, M. Kashani Maleki, M. Ghandi, Multifunctional Cu(II) organic–inorganic hybrid as a catalyst for Knoevenagel condensation, React. Kinet. Mech. Cat. 117 (2015) 87–101.
[46] H. Mahmoudi, R. Malakooti, Mn-grafted imine-functionalized mesoporous SBA-15 as an efficient catalyst for Knoevenagel condensation under mild conditions, React. Kinet. Mech. Cat. 113 (2014) 241–255.
[47] K. Koh, A.G. Wong-Foy, A.J. Matzger, MOF@MOF: microporous core-shell architectures, Chem. Commun. 6162–6164 (2009).
[48] J. Yang, H. Ye, F. Zhao, B. Zeng, A novel Cu_xO nanoparticles@ZIF-8 composite derived from core-shell metal-organic frameworks for highly selective electrochemical sensing of hydrogen peroxide, Acs Appl. Mater. Inter. 8 (2016) 20407–20414.
[49] K. Zhao, W. Wang, Z. Li, Highly efficient Ni/ZrO_2 catalysts prepared via combustion method for CO_2 methanation, J. CO_2 Util. 16 (2016) 236–244.
[50] Y. Liu, S. Zhou, J. Li, Y. Wang, G. Jiang, Z. Zhao, B. Liu, X. Gong, A. Duan, J. Liu, Y. Wei, L. Zhang, Photocatalytic reduction of CO_2 with water vapor on surface La-modified TiO_2 nanoparticles with enhanced CH_4 selectivity, Appl. Catal. B-Environ. 168–169 (2015) 125–131.
[51] Z. Fu, Y. Zhong, Y. Yu, L. Long, M. Xiao, D. Han, S. Wang, Y. Meng, TiO_2-doped CeO_2 nanorod catalyst for direct conversion of CO_2 and CH_3OH to dimethyl carbonate: catalytic performance and kinetic study, ACS Omega 3 (2018) 198–207.
[52] R. Razzaq, C. Li, M. Usman, K. Suzuki, S. Zhang, A highly active and stable Co_4 N/γ-Al_2O_3 catalyst for CO and CO_2 methanation to produce synthetic natural gas (SNG), Chem. Eng. J. 262 (2015) 1090–1098.
[53] F.X.L. i Xamena, F.G. Cirujano, A. Corma, An unexpected bifunctional acid base catalysis in IRMOF-3 for Knoevenagel condensation reactions, Micropor. Mesopor. Mat. 157 (2012) 112–117.
[54] R.S. Malkar, G.D. Yadav, Synthesis of cinnamyl benzoate over novel heteropoly acid encapsulated ZIF-8, Appl. Catal. A-Gen. 560 (2018) 54–65.
[55] I. Prymak, V.N. Kalevaru, S. Wohlrab, A. Martin, Continuous synthesis of diethyl carbonate from ethanol and CO_2 over Ce–Zr–O catalysts, Catal. Sci. Technol. 5 (2015) 2322–2331.
[56] F. Lónyi, J. Valyon, J. Engelhardt, Characterization and catalytic properties of sulfated ZrO_2–TiO_2 mixed oxides, J. Catal. 160 (1996) 279–289.
[57] T. Boningari, P.R. Ettireddy, A. Somogyvari, Y. Liu, A. Vorontsov, C.A. McDonald, P.G. Smirniotis, Influence of elevated surface texture hydrated titania on Ce-doped Mn/TiO_2 catalysts for the low-temperature SCR of NO_x under oxygen-rich conditions, J. Catal. 325 (2015) 145–155.
[58] L. Wang, W. Li, S.J. Schmieg, D. Weng, Role of Brønsted acidity in NH 3 selective catalytic reduction reaction on Cu/SAPO-34 catalysts, J. Catal. 324 (2015) 98–106.
[59] V.N. Panchenko, M.M. Matrosova, J. Jeon, J.W. Jun, M.N. Timofeeva, S.H. Jhung, Catalytic behavior of metal–organic frameworks in the Knoevenagel condensation reaction, J. Catal. 316 (2014) 251–259.
[60] Y. Yang, H.F. Yao, F.G. Xi, E.Q. Gao, Amino-functionalized Zr (IV) metal–organic framework as bifunctional acid–base catalyst for Knoevenagel condensation, J. Mol. Catal. A-Chem. 390 (2014) 198–205.
[61] F. Martínez, G. Orcajo, D. Briones, P. Leo, G. Calleja, Catalytic advantages of NH_2 -modified MIL-53(Al) materials for Knoevenagel condensation reaction, Micropor. Mesopor. Mat. 246 (2017) 43–50.
[62] A. Dhakshinamoorthy, N. Heidenreich, D. Lenzen, N. Stock, Knoevenagel condensation reaction catalysed by Al-MOFs with CAU-1 and CAU-10-type structures, Crystengcomm 19 (2017) 4187–4193.
[63] U.P.N. Tran, K.K.A. Le, N.T.S. Phan, Expanding applications of metal−organic frameworks: zeolite imidazolate framework ZIF-8 as an efficient heterogeneous catalyst for the knoevenagel reaction, Acs. Catal. 1 (2011) 120–127.
[64] M. Opanasenko, A. Dhakshinamoorthy, M. Shamzhy, P. Nachtigall, M. Horáček, H. Garcia, J. Čejka, Comparison of the catalytic activity of MOFs and zeolites in Knoevenagel condensation, Catal. Sci. Technol. 3 (2013) 500–507.
[65] S.N. Kim, S.T. Yang, J. Kim, Post-synthesis functionalization of MIL-101 using diethylenetriamine: a study on adsorption and catalysis, Crystengcomm 14 (2012) 4142–4147.
[66] J. Gascon, U. Aktay, M.D. Hernandez-Alonso, G.P.M.V. Klink, F. Kapteijn, Amino-based metal-organic frameworks as stable, highly active basic catalysts, J. Catal. 261 (2009) 75–87.
[67] M. Hartmann, M. Fischer, Amino-functionalized basic catalysts with MIL-101 structure, Micropor. Mesopor. Mat. 164 (2012) 38–43.
[68] L.T.L. Nguyen, K.K.A. Le, H.X. Truong, N.T.S. Phan, Metal–organic frameworks for catalysis: the Knoevenagel reaction using zeolite imidazolate framework ZIF-9 as an efficient heterogeneous catalyst, Catal. Sci. Technol. 2 (2012) 521–528.
[69] D. Rambabu, M. Ashraf, Pooja, A. Dhir, A. Gupta, Mn-MOF@Pi composite: synthesis, characterisation and an efficient catalyst for the Knoevenagel condensation reaction, Tetrahedron Lett. 58 (2017) 4691–4694.
[70] D. Wang, Z. Li, Bi-functional NH_2-MIL-101(Fe) for one-pot tandem photo-oxidation/Knoevenagel condensation between aromatic alcohols and active methylene compounds, Catal. Sci. Technol. 5 (2015) 1623–1628.